EES Batteries

PAPER

View Article Online
View Journal | View Issue

Cite this: *EES Batteries*, 2026, **2**, 189

Structural descriptors controlling pore-filling mechanism in hard carbon electrode during sodiation

Lincoln Mtemeri and Yue Qi *

Sodiation mechanism in hard carbons, despite their ambiguous structures, is widely understood to involve three stages: adsorption at defects and edges, intercalation between graphene layers, and nano-pore filling. Among these, nano-pore filling might be the most important sodiation stage with its characteristic low-voltage plateau (~0.1 V) observed over an extended capacity range. To investigate the pore filling mechanism, we introduce a representative nanopore model based on zeolite-templated carbon (ZTC), which consists of mainly sp^2-bonded carbon sheets curved into well-defined interconnected nanopores, facilitating well-defined pore descriptors. Three ZTC models with pore sizes of 8.8 Å, 10.1 Å, and 11.2 Å were selected to represent the ideal nanopore features in hard carbon. A pore-filling algorithm, along with density functional theory (DFT) and *ab initio* molecular dynamics (AIMD) calculations, was used to investigate the sodiation process within the nanopores. Simulations reveal that the pore filling starts from Na absorption near the carbon walls *via* ionic bonding. As Na filling progresses towards the center, the bonding character gradually transitions to more metallic. Consequently, smaller pores exhibit higher sodiation voltage than larger pores, agreeing with experimental observations. Notably, the ZTC structure with 11.2 Å pores has a plateau voltage that aligns closer to the experimentally observed 0.1 V. The theoretical capacity with favorable formation energies can reach up to NaC_3 (~470 mAh g^{-1}), more than the theoretical capacity of LiC_6. Comparing the pore filling of ZTC with carbon nanotubes suggests that the presence of non-6-carbon rings in ZTC facilitates charge transfer from Na to carbon, forming ionic bonds. Together, these descriptors – pore size, specific volume, and carbon topology offer design guidelines to quantify carbon electrode design for sodium-ion batteries.

Received 31st October 2025,
Accepted 3rd November 2025

DOI: 10.1039/d5eb00210a

rsc.li/EESBatteries

Broader context

Hard carbon (HC), the most practical anode for sodium-ion batteries (SIBs), faces dramatic development challenges because the mechanisms of sodium storage during one of its most important stages—nanopore filling—are not fully understood. The structural complexity of HC has prevented quantitative correlations between pore characteristics and the open-circuit voltage (OCV) profiles observed experimentally, limiting the ability to design materials with predictable performance.

We address this by introducing zeolite-templated carbon (ZTC) as a model system that isolates and reveals the mechanisms of sodium storage in nanopores. ZTC's curved sp^2 carbon networks form 3D interconnected pores with tunable geometry and chemistry, enabling systematic evaluation of pore descriptors.

Using a custom pore-filling algorithm with density functional theory (DFT) and *ab initio* molecular dynamics (AIMD), we predict OCV and capacity up to ~470 mAh g^{-1} during pore filling. Sodium first adsorbs ionically at pore walls before transitioning to metallic clusters at the pore center. It was quantitatively demonstrated that the ~1 nm sized connected pores formed by curved sp^2-bonded 5,6,7-membered carbon rings correspond to the experimentally observed pore filling voltage plateaus at ~0.1 V. These insights provide concrete design criteria for HC anodes and demonstrate the broader importance of rational pore engineering in energy storage materials.

1. Introduction

Sodium-ion batteries (SIB) have emerged as a viable energy storage solution for grid or transportation applications due to their advantages, such as the abundance of sodium, lower cost, and compatibility with existing lithium-based battery infrastructure.[1,2] To meet the modern capacity demands, sodium batteries must be carefully designed with high-performance intercalation materials for both electrodes.[2,3] While graphite has been the conventional anode in LIBs, it shows no intercalation preference for sodium.[4,5] Alternatively, hard carbon has emerged as a promising negative electrode for

School of Engineering, Brown University, Providence, RI 02912, USA.
E-mail: yueqi@brown.edu

sodium due to its favorable electrochemical properties.[6,7] However, sodiation mechanism of hard carbon remains poorly understood due to the complexity of hard carbon structure, which also limits theoretical models that can even quantify the open-circuit voltage (OCV).

The primary challenge in the computational modeling of hard carbon is the existence of numerous structure representations, built around the widely accepted "house of cards" analogy.[8,9] This framework characterizes hard carbon as having graphitic domains with short, uniformly stacked graphene sheets that contain defects and non-graphitic domains with curved surfaces that give rise to pore features.[10–12] Based on this model, Na storage has been proposed to fall into three regimes: (1) absorption at defects and edges, resulting in a high voltage steepest slope (1–1.5 V), (2) intercalation between layers contributing to a slope of (0.1–1 V)[13] and (3) pore-filling, which gives rise to the low voltage plateau at (0.1 V) of the discharge OCV profile.[10,14] Recent *operando* characterization techniques have revealed that the pore filling process corresponding to the ~0.1 V voltage plateau is non-uniform and highly dependent on both pore size distribution (closed/open) and defect concentration.[15] However, understanding such pore behavior through simulations remains difficult, limiting the ability to produce consistent, structure-dependent predictions.

Early Density Functional Theory (DFT) calculations have modeled the contribution of defects and the expanded graphite using simplified planar defective graphene[7,16–19] and AB-stacked layers,[5,18,19] respectively. A few studies isolated the contribution of pore storage to the overall Na storage mechanism in hard carbon. One example includes Tateyama and coworkers,[18] who simulated the pore-size effect by inserting Na clusters or slabs into the space between two parallel graphene layers and found negative formation energies in the 0.78–2 nm interlayer spacing range. Another simulation employed two tilted defective graphene layers to mimic wedge-pores and found both ionic and metallic Na inside the pore.[14] While these models provide valuable mechanistic insights, quantitative correlation of pore characteristics with the OCV and capacity has not been achieved.[20]

To investigate the role of nano-sized pores on the sodiation mechanism, we introduce a family of porous carbon structures that are synthesized from zeolite-templated carbon (ZTC).[21,22] They share similar features of carbon Schwarzites structures, such as highly sp^2 bonded carbon, negative Gaussian curvature, high porous volume, *etc*. Schwarzites structures have been proposed as part of building blocks in hard carbon, with curved fullerene-like structures.[23] These structures exhibit a well-defined three-dimensional network of interconnected nanopores with irregular geometries and topological diversity. Their features can be quantitatively described using well-defined descriptors:[24] (1) the local pore diameter, defined as the diameter of the largest sphere that can fit in a specific region without considering pore connectivity, (2) the triply periodic free sphere diameter, which represents the largest sphere that can freely move through the interconnected channels or restrictive diameter, (3) specific volume which is related to the ratio of geometric occupiable volume to the mass of carbon in the structure, (4) density, and (5) porosity. Moreover, ZTC-based pore structures are an ideal system because they feature chemically uniform carbon networks free of oxygen or hydrogen, enabling isolation and interpretation of Na–C interactions.

Moreover, templated carbon can be synthesized as a standalone carbon material for batteries and capacitors. Zeolite-templated carbon[25] and MgO-templated carbon[26] have been synthesized, with nanosized pores and sp^2 bonding characteristics, for sodium-ion batteries. Kwon *et al.*[27] and Park *et al.*[28] have synthesized ZTC for Li-ion batteries, demonstrating higher capacity than graphite. The nanoscale pore features in ZTC also facilitated their applications in aluminum batteries,[29] supercapacitors,[22,30] and catalysis.[31] Thus, unlike simplified carbon nanotubes or planar graphene-based models, ZTC-based models are not only computationally accessible, but also experimentally relevant, making them a valuable system for exploring the structure–property relationships for sodium storage.

Motivated by these structures, we aim to obtain a fundamental understanding of the structural and chemical descriptors that control the pore filling process. Such descriptors are essential for calibrating and designing hard carbon materials to enhance the energy density of sodium-ion batteries (higher capacity and lower voltage). To this end, we first developed a pore-filling algorithm that incrementally inserts sodium atoms into the occupiable pore space, up to saturation. A combination of DFT minimization and *ab initio* molecular dynamics (AIMD) simulations was used to sample thermodynamically stable structures. The formation energies were then analyzed *via* a convex hull construction, followed by calculations of the open-circuit voltage (OCV) profiles.

The OCV plateaus predicted by these structures were compared with available experimental observations showing pore sodiation. Additionally, the charge states of Na atoms were examined to reveal the pore filling mechanism and bonding nature. Finally, our pore-filling results were evaluated against nanotube and slab models to further correlate the structural and chemical descriptors that determine the pore filling capacity and voltage.

2. Computational methods

2.1 ZTC structures and pore characteristics

ZTC-based pore structures were obtained from the ToposPro database.[21] These structures were originally generated from a zeolite template sourced from the IZA database.[32] The process employs a Monte Carlo (MC) algorithm that loads sp^2-hybridized carbon atoms onto zeolite surfaces, followed by DFT minimization. This approach mimics the synthetic process, which involves the formation of a carbon network conformal on the pore surface in zeolite, resulting carbon loading levels comparable to those achievable through experimental synthesis.[33,34]

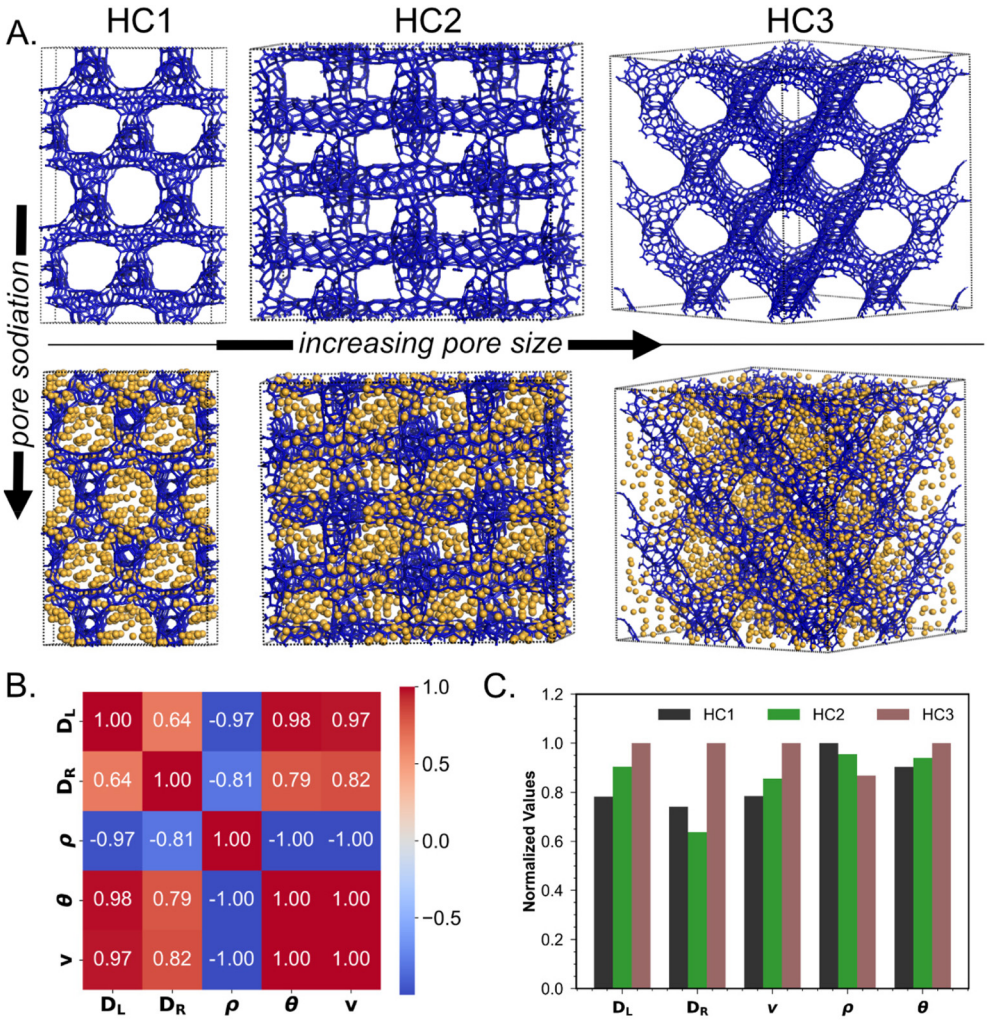

Fig. 1 Characterization of three pore structures. (A) Atomistic representation of three distinct 3D nanopore networks and connectivity shown in 2 × 2 × 2 supercells before and after sodiation. Na atoms are shown in yellow and C in blue. (B) Spearman correlation matrix showing interdependencies between properties. (C) Quantitative analysis of pore topology, including local diameter (D_L), restrictive diameter (D_R), specific volume (ν), density (ρ), and porosity (θ).

From this set, three representative pore models were selected and labeled **HC1**, **HC2** and **HC3** as shown in Fig. 1A. Our selection criterion mainly focused on (i) well-defined 3D-nanopore network composed of sp^2-hybridized carbon atoms arranged in polycyclic rings, (ii) the presence of multiple atom bridges connecting pore walls to enhance structural rigidity and pore confinement, and (iii) distinct pore characters that enable systematic comparison.

The structures were analyzed to determine their pore characteristics using Zeo++ software package[35] and the Connolly surface method[36] in Materials Studio programs. Zeo++ [35] was employed to calculate key topological features of the crystalline porous structures. This algorithm uses Voronoi/Delaunay decomposition and Monte Carlo integration[37] to extract geometric characteristics, including the local pore diameter (D_L), which represents the largest occupiable space; and the restrictive diameter (D_R), which characterizes the narrowest part of a pore channel. The geometric occupiable volume (V_g), which quantifies the space that is accessible to a fluid or gas, is directly related to porosity (θ) as the ratio of void space to the total volume. The specific volume (ν), which is the inverse of density (ρ), represents the volume normalized by mass. These characteristics are shown in Fig. 1C. To validate the Zeo++ results, the Connolly surface method was used to calculate the pore volume using a probing radius of 1.8 Å and achieved comparable results to those obtained from Zeo++ program, as shown in Table S1. More details about the program implementation are in the SI.

2.2. Sodium insertion algorithm and computational details

A python-based algorithm was developed to sequentially fill the pore space with Na atoms at various concentrations. The algorithm employed a Voronoi/Delaunay decomposition framework to identify and fill the occupiable pore volume in

the structures. Expanding the unit cell along different directions further checks the identification of connected voids across periodic boundaries, while the original unit cell with Na was used in all DFT calculations. Voronoi tessellation was then applied to locate pore centers. Na atoms were inserted into the pore space, starting near the carbon walls and extending towards the center, following the energetics sequence tested by individual occupancy as a function of distance to the wall (Fig. S1). While filling the space, the initial distance between Na–C and Na–Na was set to be 2.4 Å and 3.0 Å, respectively, following their general bond distance. At least 2 to 3 configurations were generated for each Na composition. These initial configurations were minimized *via* DFT calculations. The RDFs of C–C, Na–C and Na–Na pairs in **HC1** are shown in Fig. S2, comparing empty and filled structures to demonstrate that the carbon framework is maintained after full sodiation.

This pore filling algorithm led to structures with slightly lower energies than an earlier version with a less controlled filling procedure. To validate the stability of the resulting compositions, representative structures with the lowest energy at selected concentrations (*e.g.*, Na = 5, 10, 15 ... *etc.*) up to saturation, were extracted, especially for **HC3**, and AIMD simulations were conducted to investigate their energy evolution over time.

All DFT calculations were performed using the plane-wave-based Vienna *Ab initio* Simulation Package (VASP) code.[38] The Projector Augmented Wave (PAW) method was employed in conjunction with the Perdew–Burke–Ernzerhof (PBE) exchange–correlation functional. No dispersion correction was applied because ZTC is dominated by covalently bonded carbon, instead of layered graphite bonded by van der Waals forces. This choice is supported by the energy per atom comparison, with and without dispersion correction, shown in Table S3. Brillouin zone sampling was restricted to the Gamma point (1 × 1 × 1 *k*-point mesh). The plane-wave cutoff energy was set to 600 eV. The electronic energy convergence criterion was 1×10^{-6} eV per atom, and the force convergence threshold was set to 0.02 eV A^{-1}. Geometry optimizations were carried out with fixed unit cell shape and volume, allowing only atomic positions to relax. AIMD simulations were performed by employing the Nosé–Hoover thermostat within an *NVT* ensemble (constant number of particles, volume, and temperature) to maintain thermal equilibrium at 298 K. A time step of 1 fs was used, and each trajectory was propagated for 10 000 steps (10 ps total duration), sufficient to assess local stability and atomic fluctuations. The lowest energy structure was extracted from the trajectory for subsequent energy minimization and further analysis.

2.3 Thermodynamic analysis of formation energy and OCV

The sodiation process in hard carbon can be described using the form $y\mathrm{Na} + (1-y)\mathrm{C} \rightarrow \mathrm{Na}_y\mathrm{C}_{1-y}$, where y is the mole fraction defined as:

$$y = \frac{N_{\mathrm{Na}}}{N_{\mathrm{Na}} + N_{\mathrm{C}}} = \frac{x}{1+x},$$

with N_{Na} and N_{C} being the number of Na and C atoms in the structure, respectively. The stoichiometry of the structure is often written as $\mathrm{Na}_x\mathrm{C}$. The formation energy for $\mathrm{Na}_x\mathrm{C}$, E_{f}, is given as:

$$E_{\mathrm{f}}(\mathrm{Na}_x\mathrm{C}) = E_{\mathrm{Na}_x\mathrm{C}} - (1-y)\cdot E_{\mathrm{C}} - y \cdot E_{\mathrm{Na,BCC}}, \quad (1)$$

where $E_{\mathrm{Na}_x\mathrm{C}}$, E_{C} and $E_{\mathrm{Na,BCC}}$ are the energies per atom of the pore-filled, empty carbon host and Na BCC crystal phases. The sodiation open-circuit voltage, V, is defined by the change in Gibbs free energy:[39,40]

$$V = -\frac{\Delta G}{\Delta x}$$

with respect to the sodiation concentration change, Δx. $\Delta G = \Delta E + P\Delta V - T\Delta S$. The term $P\Delta V$ and $T\Delta S$ are negligible for solid state reactions at room temperature. Therefore, the voltage expression is reduced to:

$$\begin{aligned} V(x+\Delta x, x) &= -\frac{\Delta E_{\mathrm{f}}}{\Delta x} = -\frac{E_{\mathrm{f}}(\mathrm{Na}_{(x+\Delta x)}\mathrm{C}) - E_{\mathrm{f}}(\mathrm{Na}_x\mathrm{C})}{\Delta x} \\ &= -\frac{E_{\mathrm{Na}_{x+\Delta x}\mathrm{C}} - E_{\mathrm{Na}_x\mathrm{C}} - \Delta x E_{\mathrm{Na,BCC}}}{\Delta x} \end{aligned} \quad (2)$$

The term, Δx is calculated from $\Delta x = x_i - x_{i-1}$, where x_i and x_{i-1} are the current and previous Na content at each intercalation stage. Eqn (1) and (2) were employed to compute the convex hull formation energies and corresponding sodiation voltages.

3. Results and discussion

3.1 ZTC structures and descriptors

The selected ZTC-based structures exhibit ideal pore characteristics that closely mimic the porous morphology desired in hard carbon electrodes. These models were chosen because of their well-defined, 3D interconnected nanopores, which vary in size and geometry as defined by the descriptors shown in Fig. 1 and Table S1. Although the pores are irregular and non-spherical, they are structurally supported by multiple carbon ring linkages that preserve periodicity across the framework.

The pore characteristics were compared using a Spearman correlation matrix to show the interdependencies among the pore features. For example, local pore diameter (D_{L}) showed a strong positive correlation with both porosity and specific volume, and a negative correlation with density (magnitude of correlation coefficients >0.95) (Fig. 1B). This suggests a direct relationship between pore size and overall structural compactness. Moreover, these descriptors point to promising Na storage due to the presence of accessible filling space. The restrictive diameter (D_{R}), which reflects the size of the largest sphere that can percolate through the interconnected void space, follows the same trend as the local pore diameter, but shows a weaker positive correlation with porosity and specific volume (with coefficients in the 0.6 and 0.7 range). In this study, D_{L} is the strongest descriptor of pore size, while the D_{R} is relevant in the context of ion transport.

Among the selected structures, the pore characteristics exhibit variations as shown in Fig. 1C. Collectively, the density, porosity, and specific volume serve as key indicators of atom packing efficiency and the amount of accessible void space within each structure. The pore size increases progressively from **HC1** to **HC3**, as indicated by monotonically increasing local pore diameter (D_L), specific volume (ν), and porosity (θ).

3.2 Formation energy and OCV prediction

Sodiation of the three ZTC pore structures results in negative formation energies with respect to ZTC and metallic Na in most of Na-filled structures, computed using eqn (1) (Fig. 2A and Fig. S3). Points on the convex hull further indicate phase stability. The low energy configurations for **HC1** and **HC2** closely follow the convex hull, indicating a continuous sodiation process. The minimized structures in **HC3** appear to have more compositions above the convex hull. Further minimization of low energy structures obtained from their AIMD trajectory shows formation energies in the range of ~0.01 eV per atom; on the same order as the formation energy itself. Given these fluctuations, sodiation of **HC3** is likely to follow a continuous path rather than distinct phase transitions.

The sodiation saturation composition can be determined from the convex hull, where the formation energies increase sharply above the tie line connecting to the sodium metal. This means further sodium insertion will lead to sodium metal precipitation. For all three ZTC structures, the saturation stoichiometry is in the range of y = 0.25–0.28, corresponding to NaC_3, which is significantly higher than previously predicted stable Na–C phases such as NaC_8 in defective graphene,[7] NaC_{16} in wedge and slab structures[17,18] or NaC_{48}, NaC_{64} and NaC_{80} in graphitic domains.[41] This level of sodiation capacity has been reported in ZTC[26] and hard carbons tailored with nanometer pores.[42] More interestingly, experimentally tested ZTC also shows capacities surpassing the lithiated graphite LiC_6.[27] These results highlight the favorable sodium storage potential of the ZTC-based modeled pore structures compared to conventional planar graphite sheets.

Among the three ZTC structures, **HC1** exhibits the most negative formation energy, following the stability trend **HC1** > **HC2** > **HC3**. Consequently, the DFT predicted OCV from the convex hull points also decreases in the same sequence, especially in the voltage plateaus corresponding to the last stage of sodiation (Fig. 2B and Fig. S4). These sodiation

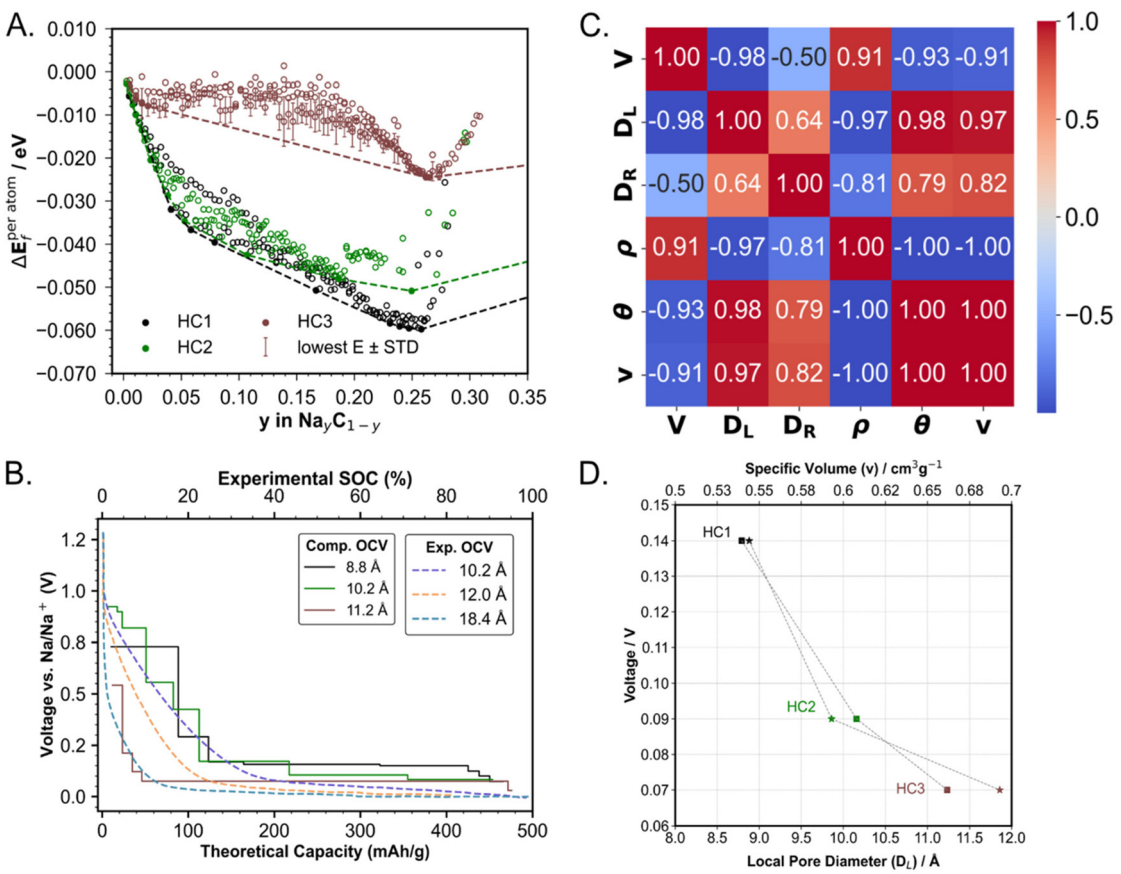

Fig. 2 Calculated results for sodium pore filling: (A) formation energies and corresponding convex hull; (B) open-circuit voltage profile, with piecewise steps (solid lines) representing voltages derived from convex hull vertices and smooth curves (dotted lines) representing voltages experimentally obtained; (C) Spearman correlation matrix showing the correlation of pore features with plateau voltage; (D) relationship between local pore diameter and specific volume with the observed pore-filling voltage plateau analyzed at capacity of 409 mAh g^{-1}.

voltage plateaus directly correlate with key pore descriptors, which are pore diameter, specific volume, and porosity (Fig. 2C and D) and decrease monotonically as each of these parameters increases. Conversely, since density is the inverse of specific volume, the plateau voltage rises with the density of ZTC structures. Together, these trends demonstrate that pore size and packing density play a direct role in controlling the voltage profiles.

Comparison of our predicted OCV profiles with available experimental data further supports the key trends captured by the ZTC model. Toney and co-workers[15] synthesized HC structures *via* pyrolysis at different temperatures (1100 °C, 1400 °C, and 2000 °C) and characterized the resulting pore diameters within a similar range to our simulations. Their experimental measurements yielded mean pore radii of 5.1 Å, 6.0 Å, and 9.2 Å, respectively, increasing with pyrolysis temperatures (Fig. S5). Upon electrochemical measurements, the results showed that HCs prepared at lower pyrolysis temperatures exhibited smaller pore size and higher voltage plateaus compared to those synthesized at higher temperatures. Our ZTC model shows similar key trends: (1) the high voltage plateau associated with the small pores and the lower voltage closer to ~0.1 V associated with larger pores (Fig. 2B), (2) the gradual sloping region and its extended plateau. These results suggest that ZTC-based structures can reliably represent the nanopore-dependent electrochemical characteristics of hard carbon and can serve both as representative model systems for understanding storage behavior and as viable anode materials for Na-ion batteries.

3.3 Chemical bonding during pore filling

To further understand the origin of the voltage and pore size relationship, we analyzed the bonding nature of sodium during the sodiation process. Bader charge analysis was performed at various Na contents (*e.g.*, N_{Na} = 5, 10, 15, ... N_x, where N_x represents the maximum capacity of each structure). For illustration, we compared low and high Na concentrations in **HC1**, specifically $Na_{0.02}C$ and $Na_{0.35}C$, to visualize the Bader charges on each atom in these two structures. At low concentration, $Na_{0.02}C$, sodium atoms exhibit charges close to +1 (appearing reddish), indicating the strong ionic bonds with the carbon walls (Fig. 3A). Even at higher concentration ($Na_{0.35}C$), Na atoms near the carbon surface (orange to yellow atoms) show relatively high positive charges, reflecting the persistent ionic bonding. In comparison, Na atoms closer to the pore center have lower charge states (appearing as greener to bluish colors), reflecting a more metallic bonding character.

More broadly, Bader charge analysis across all structures reveals a range of charge states. As pore-filling progresses, a transition from ionic to metallic character is observed (Fig. 3B). When the average Bader charge at the voltage plateau is evaluated against the Na : C ratio, another trend emerges; structures that accommodate lesser sodium (lower Na : C atomic ratios) exhibit stronger ionic character. In other words, the decrease in average Bader charge with increasing Na : C ratio also reflects a transition from ionic Na–C interactions to metallic Na–Na clustering within the pores.

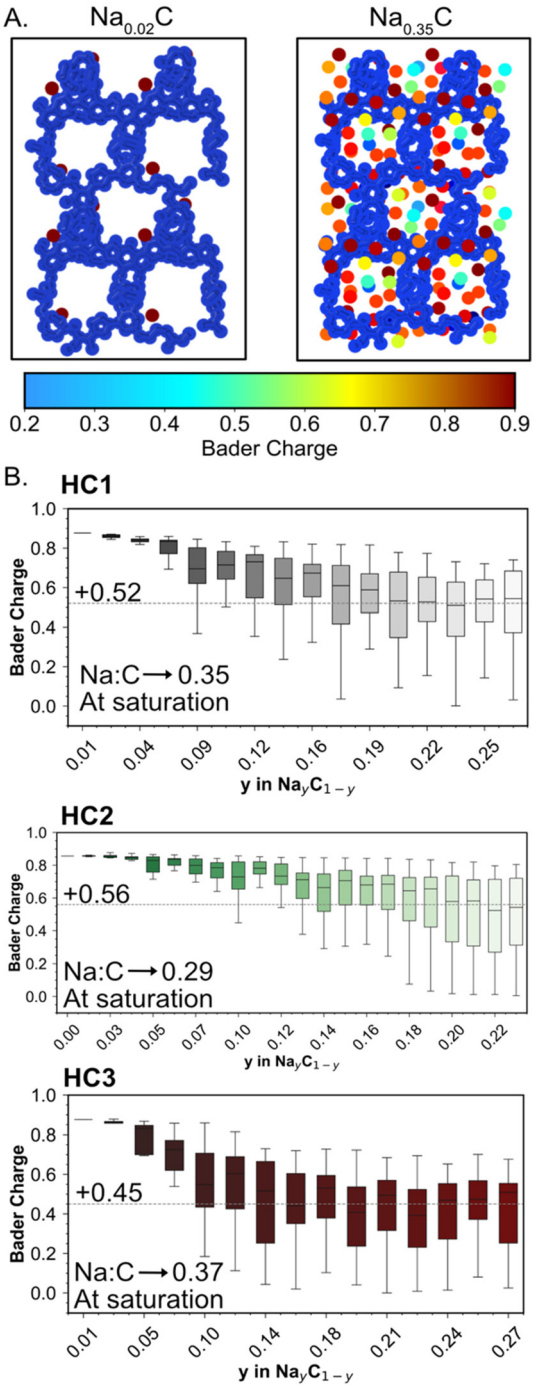

Fig. 3 Bader charge analysis. (A) Visual representation of Na atom charge states in filled **HC1**, shown as a color gradient. Atoms near the carbon walls (in blue) appear more reddish, yellowish or orange, indicating higher ionicity; while atoms closer to the center appear greener or light blue to represent more metallic character. (B) The distributions of charges sampled at the respective Na contents illustrate the progressive transition from ionic to metallic as content increases. The horizontal lines represent the charge plateau reached at saturation.

The stronger ionic Na–C interactions give rise to the more negative formation energy and higher OCV, while the metallically bonded Na atoms result in voltages closer to zero. Thus,

smaller pores favor ionic bonding, which elevates the voltage, whereas excessively large pores promote metallic bonding, resulting in a voltage drop toward zero. The intermediate plateau voltage observed in these systems is consistent with a mixed bonding character. Overall, this trend suggests that as pore diameter increases, the bonding environment shifts toward metallic, resulting in a gradual reduction in OCV. Therefore, the pore size and Na : C ratio must be carefully optimized to maintain the desired electrochemical performance. Specifically, pores with diameters in the range of ~10 Å appear to sustain a voltage plateau closer to 0.1 V.

This mechanistic interpretation aligns well with prior studies of sodium clusters in graphitic planes,[18] wedge pores or slits[14] and disorder nanoporous carbon,[43] which have consistently shown that smaller pores promote ionic bonding and high voltage, while larger pores favor metallic bonding with lower charge states. An important advancement is that the ZTC model predicted the pore filling voltage plateau and capacity that are consistent with the experimental data, which could not be achieved by previous carbon models. Thus, the ZTC model unified the previous understanding obtained from idealized graphite or CNTs structures with more realistic nanopore structures.

3.4 Comparison of pore model, nanotube and planar graphene

The effectiveness of the current ZTC pore structure arises from the presence of 3D interconnected channels bounded by curved carbon walls. Unlike flat graphene-based models, this type of pore architecture provides additional pore characteristics and chemical features that enhance sodium storage.

Planar graphite models have been previously studied,[14,18] primarily to examine the effects of interlayer spacing on sodium formation energies. However, these planar systems show limited capacity, typically plateauing at compositions like Na_{10} hosted between 72- to 128-carbon atom sheets. In contrast, pore filling, especially in the range of ~10 Å diameter, can provide more storage. Nevertheless, pore volume alone does not fully account for the observed intercalation capacity.

To further explore this, we compared the pore models with a sodiated nanotube featuring a local diameter of 11.5 Å, a unit cell length of 15 Å and a resulting specific pore volume of 0.28 $cm^3\ g^{-1}$ as illustrated in Fig. 4. The results show that the

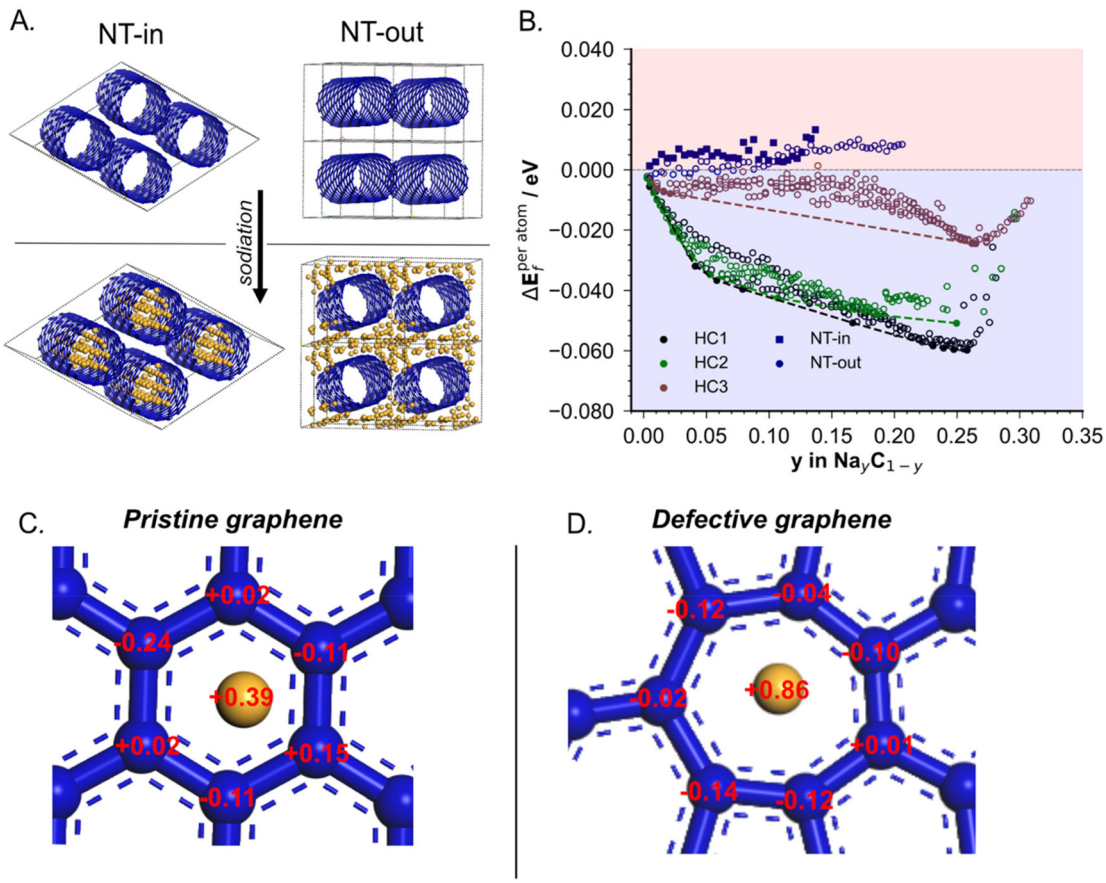

Fig. 4 Sodiation of a nanotube structure compared to representative pore models. (A) Visualization of the nanotube in its empty and fully sodiated state up to $Na_{35}C_{208}$, with a diameter of 11.5 Å. (B) Convex hull plot of formation energies, showing that the NT configurations lie in the positive region, indicating thermodynamic instability relative to pore-based structures. C and D show adsorption geometries comparing Na atom Bader charges next to a planar six-membered ring and a nonplanar seven-membered ring, respectively. The formation energies are 0.027 eV per atom in pristine graphene and −0.038 eV per atom in defective graphene.

nanotube has no thermodynamic preference for sodiation as demonstrated by the positive formation energies. This observation is consistent with previous findings, as a nanotube is essentially a rolled graphene sheet, which has been known to have no early-stage Na intercalation.[5,16,18]

Further analysis of the Bader charge distribution (Fig. S6) indicates that the average charge associated with the nanotube during sodiation is lower than that observed in all ZTC pore structures. The carbon atoms in the nanotube remain closer to a neutral charge state, suggesting weaker Na–C interactions relative to the ZTC pore models. This weak interaction promotes a more quasi-metallic or near-neutral character of Na within the nanotube, which is unfavorable for efficient charge storage. In contrast, the ZTC pore structures exhibit a mixed ionic–metallic behavior, which facilitates stronger Na–C interactions.

The presence of a mix of non-planar 5-, 7-, 8- C-rings plays a crucial role in establishing favorable C–Na interactions, promoting effective pore-filling and enhancing sodium storage. These non-planar rings exhibit negative formation energies. A simplified model of Na atom adsorption on pristine and defective graphene sheets highlights the difference (Fig. 4C and D). In contrast to flat aromatic systems, the geometric deviation from planarity (pyramidalization) disrupts π-conjugation and creates localized sites that can accept electron density from sodium. The partial sp^3 character in strained rings also increases polarizability,[19] making it easier for Na to ionize. This behavior is evident in the Bader charge comparison shown in Fig. 4C, where the Na^+ in planar carbon rings exhibits a quasi-metallic character (+0.39), compared to a more ionic state (+0.86) in defective rings, highlighting the distinct Na–C interaction chemistries. This explains the fundamental difference between the pores in ZTC and carbon nanotubes. Similar findings have been reported for lithium: Li binding to perfect graphene is endothermic, while defects promote exothermic Li adsorption due to enhanced electron localization.[44]

While earlier studies on defective graphene proxies emphasized charge transfer resulting from the breaking of the C6 unit in a planar network, our model introduces a structurally distinct framework, a 3D-connected nanopore system with hexagonal and non-hexagonal rings in ZTC. It allows accurate prediction of the voltage and capacity of sodiation into the pores.

Finally, this research addresses an ongoing discussion in the literature regarding the role of closed *versus* open pores in hard carbon matrices. While closed pores are often favored due to their ability to create confined active sites for Na-ion storage,[14] they have limitations. In a typical pore distribution, many closed pores remain unfilled, and pore filling tends to occur non-uniformly, particularly for larger-radius pores, due to the absence of accessible pathways to these unutilized regions.[15] Moreover, closed pores may restrict the transport of solvated Na-ions, which is essential for efficient battery operation. Based on our findings, we propose that the semi-open pore structures, those that are interconnected, can offer a balanced advantage by supporting favorable bonding, storage capacity and ion transport, making them attractive candidates in sodium-ion battery applications.

4. Conclusion

This work addresses a challenge in both theoretical modeling and practical hard carbon design, which is the lack of adequate models capable of quantifying pore sodiation and predicting its contribution to the open-circuit voltage (OCV) profile. We introduce a porous carbon framework derived from zeolite-templated carbon (ZTC) to isolate and investigate the electrochemical behavior associated with nano-pore-filling in hard carbon, and to obtain practical system-level design parameters relevant for hard carbon anodes. Using a custom-designed algorithm to simulate sodium insertion into ZTC pores, we generated sodiated structures and examined their thermodynamic stability *via* atomistic simulations. Our findings demonstrate that ZTC exhibits favorable Na storage properties, as shown by negative formation energies up to NaC_3 (470 mAh g^{-1}) and consistent OCV values with experiments that outperform other carbon models such as graphene with slits and nanotubes. A key insight from this study is the evolution of Na–C bonding during pore filling. Initially, Na atoms bind ionically closer to the carbon pore walls. As sodiation progresses, the Na atoms gradually occupy the center of the pore, transitioning from ionic to more metallic bonding. The predicted OCV correlates with pore features such as specific volume and local pore diameter. Smaller pores are associated with higher voltages due to stronger ionic interactions, while larger pores promote metallic bonding, driving the voltage towards zero. Bader charge analysis supports this bonding transition, where highly positive Na charge states at low concentrations (indicative of ionic character) progressively plateaued to more neutral values as Na concentration increased, signaling metallic behavior. As a result, a pore diameter of approximately ~10 Å was found to give ideal voltage at the extended plateau of 0.1 V. Furthermore, our results also emphasize that these favorable ZTC electrochemical properties are controlled by the nature of the C bounding them. Specifically, a non-6 C membered ring facilitates ideal charge transfer compared to pristine hexagonal carbon frameworks. This underscores the roles of both geometric and electronic descriptors: pore size, specific volume and carbon topology in controlling sodiation. Overall, ZTC emerges as a powerful model system for understanding pore-dependent sodium storage in hard carbon and also as a viable material platform for designing high-performance Na-ion battery anodes with well-controlled and tunable pore features.

Conflicts of interest

The authors have no conflicts to disclose.

Data availability

The data that support the findings of this study are available from the corresponding author upon reasonable request. The

key atomic structures are provided in Supplemental Information 2.0.

Supplementary information (SI) is available. The SI2 file includes the geometric coordinates of representative structures used in this study. See DOI: https://doi.org/10.1039/d5eb00210a.

Acknowledgements

We thank NASA for financial support (grant no. 80NSSC24M0140) and the Center for Computation and Visualization at Brown for providing computational resources. L. M. was grateful for the support of the Presidential Postdoctoral Fellowship at Brown University.

References

1 J.-Y. Hwang, S.-T. Myung and Y.-K. Sun, Sodium-Ion Batteries: Present and Future, *Chem. Soc. Rev.*, 2017, **46**(12), 3529–3614, DOI: 10.1039/c6cs00776g.

2 C. Delmas, Sodium and Sodium-Ion Batteries: 50 Years of Research, *Adv. Energy Mater.*, 2018, **8**(17), 1703137, DOI: 10.1002/AENM.201703137.

3 M. Sawicki and L. L. Shaw, Advances and Challenges of Sodium Ion Batteries as Post Lithium Ion Batteries, *RSC Adv.*, 2015, **5**(65), 53129–53154, DOI: 10.1039/C5RA08321D.

4 M. S. Dresselhaus and G. Dresselhaus, Intercalation Compounds of Graphite, *Adv. Phys.*, 2002, **51**(1), 1–186, DOI: 10.1080/00018730110113644.

5 H. Moriwake, A. Kuwabara, C. A. J. Fisher and Y. Ikuhara, Why Is Sodium-Intercalated Graphite Unstable?, *RSC Adv.*, 2017, **7**(58), 36550–36554, DOI: 10.1039/c7ra06777a.

6 N. Sun, J. Qiu and B. Xu, Understanding of Sodium Storage Mechanism in Hard Carbons: Ongoing Development under Debate, *Adv. Energy Mater.*, 2022, **12**(27), 2200715, DOI: 10.1002/AENM.202200715.

7 P.-C. Tsai, S.-C. Chung, S.-K. Lin and A. Yamada, Ab Initio Study of Sodium Intercalation into Disordered Carbon, *J. Mater. Chem. A*, 2015, **3**(18), 9763–9768, DOI: 10.1039/c5ta01443c.

8 J. R. Dahn, W. Xing and Y. Gao, The "Falling Cards Model" for the Structure of Microporous Carbons., *Carbon*, 1997, **35**(6), 825–830, DOI: 10.1016/S0008-6223(97)00037-7.

9 D. A. Stevens and J. R. Dahn, High Capacity Anode Materials for Rechargeable Sodium-Ion Batteries, *J. Electrochem. Soc.*, 2000, **147**(4), 1271, DOI: 10.1149/1.1393348/XML.

10 D. Chen, W. Zhang, K. Luo, Y. Song, Y. Zhong, Y. Liu, G. Wang, B. Zhong, Z. Wu and X. Guo, Hard Carbon for Sodium Storage: Mechanism and Optimization Strategies toward Commercialization, *Energy Environ. Sci.*, 2021, 2244–2262, DOI: 10.1039/d0ee03916k, Royal Society of Chemistry.

11 Z. Lu, H. Yang, Y. Guo, H. Lin, P. Shan, S. Wu, P. He, Y. Yang, Q. H. Yang and H. Zhou, Consummating Ion Desolvation in Hard Carbon Anodes for Reversible Sodium Storage, *Nat. Commun.*, 2024, **15**(1), 3497–3510, DOI: 10.1038/s41467-024-47522-y.

12 J. M. Stratford, P. K. Allan, O. Pecher, P. A. Chater and C. P. Grey, *Chem. Commun.*, 2016, **52**, 12430, DOI: 10.1039/c6cc06990h.

13 S. Qiu, L. Xiao, M. L. Sushko, K. S. Han, Y. Shao, M. Yan, X. Liang, L. Mai, J. Feng, Y. Cao, X. Ai, H. Yang and J. Liu, Manipulating Adsorption–Insertion Mechanisms in Nanostructured Carbon Materials for High-Efficiency Sodium Ion Storage, *Adv. Energy Mater.*, 2017, **7**(17), 1700403, DOI: 10.1002/aenm.201700403.

14 Y. Li, A. Vasileiadis, Q. Zhou, Y. Lu, Q. Meng, Y. Li, P. Ombrini, J. Zhao, Z. Chen, Y. Niu, X. Qi, F. Xie, R. van der Jagt, S. Ganapathy, M. M. Titirici, H. Li, L. Chen, M. Wagemaker and Y. S. Hu, Origin of Fast Charging in Hard Carbon Anodes, *Nat. Energy*, 2024, **9**(2), 134–142, DOI: 10.1038/s41560-023-01414-5.

15 I. L. Kitsu, E. N. Antonio, T. D. Martinez, L. Zhang, Z. Zhuo, S. J. Weigand, J. Guo and M. F. Toney, Revealing the Sodium Storage Mechanisms in Hard Carbon Pores, *Adv. Energy Mater.*, 2023, **13**(44), 2302171, DOI: 10.1002/aenm.202302171.

16 D. Datta, J. Li and V. B. Shenoy, Defective Graphene as a High-Capacity Anode Material for Na- and Ca-Ion Batteries, *ACS Appl. Mater. Interfaces*, 2014, **6**(3), 1788–1795, DOI: 10.1021/am404788e.

17 K. Nobuhara, H. Nakayama, M. Nose, S. Nakanishi and H. Iba, First-Principles Study of Alkali Metal-Graphite Intercalation Compounds, *J. Power Sources*, 2013, **243**, 585–587, DOI: 10.1016/j.jpowsour.2013.06.057.

18 Y. Youn, B. Gao, A. Kamiyama, K. Kubota, S. Komaba and Y. Tateyama, Nanometer-Size Na Cluster Formation in Micropore of Hard Carbon as Origin of Higher-Capacity Na-Ion Battery, *npj Comput. Mater.*, 2021, **7**(1), 48, DOI: 10.1038/s41524-021-00515-7.

19 H. Yu, Z. Yi, W. Jia, W. Hou, L. Xie, Z. Wang, J. Chen, F. Su, D. Jiang and C. M. Chen, Confinement-Induced Stability Evolution of Na Clusters in Closed Pores of Hard Carbon: A DFT and AIMD Study, *J. Phys. Chem. A*, 2025, **129**(14), 3231–3241, DOI: 10.1021/ACS.JPCA.5C00209.

20 C. Bommier, T. W. Surta, M. Dolgos and X. Ji, New Mechanistic Insights on Na-Ion Storage in Nongraphitizable Carbon, *Nano Lett.*, 2015, **15**(9), 5888–5892, DOI: 10.1021/acs.nanolett.5b01969.

21 E. Braun, Y. Lee, S. M. Moosavi, S. Barthel, R. Mercado, I. A. Baburin, D. M. Proserpio and B. Smit, Generating Carbon Schwarzites via Zeolite-Templating, *Proc. Natl. Acad. Sci. U. S. A.*, 2018, **115**(35), E8116–E8124, DOI: 10.1073/PNAS.1805062115.

22 H. Nishihara and T. Kyotani, Templated Nanocarbons for Energy Storage, *Adv. Mater.*, 2012, **24**(33), 4473–4498, DOI: 10.1002/ADMA.201201715.

23 S. J. Townsend, T. J. Lenosky, D. A. Muller, C. S. Nichols and V. Elser, Negatively Curved Graphitic Sheet Model of Amorphous Carbon, *Phys. Rev. Lett.*, 1992, **69**(6), 921–924, DOI: 10.1103/PhysRevLett.69.921.

24 D. Ongari, P. G. Boyd, S. Barthel, M. Witman, M. Haranczyk and B. Smit, Accurate Characterization of the Pore Volume in Microporous Crystalline Materials, *Langmuir*, 2017, **33**(51), 14529–14538, DOI: 10.1021/acs.langmuir.7b01682.

25 S. Tan, C. Wang, Y. Foucaud, M. Badawi, H. Guo, K. Sun, G. Yang and S. Mintova, Ordered Sodium Zeolite-Templated Carbon with High First Discharge Capacity for Sodium Battery Application, *Microporous Mesoporous Mater.*, 2022, **336**, 111853, DOI: 10.1016/J.MICROMESO.2022.111853.

26 A. Kamiyama, K. Kubota, D. Igarashi, Y. Youn, Y. Tateyama, H. Ando, K. Gotoh and S. Komaba, MgO-Template Synthesis of Extremely High Capacity Hard Carbon for Na-Ion Battery, *Angew. Chem., Int. Ed.*, 2021, **60**(10), 5114–5120, DOI: 10.1002/ANIE.202013951.

27 Y. Kwon, K. Kim, H. Park, J. W. Shin and R. Ryoo, Anomalously High Lithium Storage in Three-Dimensional Graphene-like Ordered Microporous Carbon Electrodes, *J. Phys. Chem. C*, 2018, **122**(9), 4955–4962, DOI: 10.1021/ACS.JPCC.8B00081.

28 H. Park, R. K. Bera, H. Yoon and K. Kim, 3D Graphene-like Microporous Carbon for Ultralong-Life Lithium-Ion Capacitors, *ACS Appl. Energy Mater.*, 2025, **30**, 9489–9496, DOI: 10.1021/acsaem.5c01138.

29 N. P. Stadie, S. Wang, K. V. Kravchyk and M. V. Kovalenko, Zeolite-Templated Carbon as an Ordered Microporous Electrode for Aluminum Batteries, *ACS Nano*, 2017, **11**(2), 1911–1919, DOI: 10.1021/ACSNANO.6B07995.

30 Z. Wang, T. Wu, L. Zeng, J. Peng, X. Tan, D. Yu, M. Gao and G. Feng, Machine Learning Relationships Between Nanoporous Structures and Electrochemical Performance in MOF Supercapacitors, *Adv. Mater.*, 2025, **37**(15), 2500943, DOI: 10.1002/adma.202500943.

31 S. F. Rastegar, R. Pilar, J. Moravkova, G. Sadovska, V. I. Parvulescu, J. Pastvova, J. Plsek, D. Kaucky, N. Kostkova and P. Sazama, Platinum Nanoparticles on 3D Graphene-like Zeolite-Templated Carbon for Benzene Hydrogenation, *Catal. Sci. Technol.*, 2023, **13**(17), 5120–5130, DOI: 10.1039/D3CY00617D.

32 *Database of Zeolite Structures*. https://www.iza-structure.org/databases/ (accessed 2025-04-23).

33 H. Nishihara, H. Fujimoto, H. Itoi, K. Nomura, H. Tanaka, M. T. Miyahara, P. A. Bonnaud, R. Miura, A. Suzuki, N. Miyamoto, N. Hatakeyama, A. Miyamoto, K. Ikeda, T. Otomo and T. Kyotani, Graphene-Based Ordered Framework with a Diverse Range of Carbon Polygons Formed in Zeolite Nanochannels, *Carbon*, 2018, **129**, 854–862, DOI: 10.1016/j.carbon.2017.12.055.

34 K. Nueangnoraj, H. Nishihara, K. Imai, H. Itoi, T. Ishii, M. Kiguchi, Y. Sato, M. Terauchi and T. Kyotani, Formation of Crosslinked-Fullerene-like Framework as Negative Replica of Zeolite y, *Carbon*, 2013, **62**, 455–464, DOI: 10.1016/j.carbon.2013.06.033.

35 *Zeo++ – High throughput analysis of crystalline porous materials*. https://www.zeoplusplus.org/(accessed 2025-04-23).

36 H. L. Connoh, *Analytical Molecular Surface Calculation*, 1983, vol. 548.

37 T. F. Willems, C. H. Rycroft, M. Kazi, J. C. Meza and M. Haranczyk, Algorithms and Tools for High-Throughput Geometry-Based Analysis of Crystalline Porous Materials, *Microporous Mesoporous Mater.*, 2012, **149**(1), 134–141, DOI: 10.1016/j.micromeso.2011.08.020.

38 G. Kresse and J. Furthmüller, Efficiency of *Ab initio* Total Energy Calculations for Metals and Semiconductors Using a Plane-Wave Basis Set, *Comput. Mater. Sci.*, 1996, **6**(1), 15–50, DOI: 10.1016/0927-0256(96)00008-0.

39 V. L. Chevrier and J. R. Dahn, First Principles Model of Amorphous Silicon Lithiation, *J. Electrochem. Soc.*, 2009, **156**(6), A454, DOI: 10.1149/1.3111037.

40 A. Urban, D. H. Seo and G. Ceder, Computational Understanding of Li-Ion Batteries, *npj Comput. Mater.*, 2016, **2**(1), 16010, DOI: 10.1038/npjcompumats.2016.2.

41 A. Metrot, D. Guerard, D. Billaud and A. Herold, New Results about the Sodium-Graphite System, *Synth. Met.*, 1980, **1**(4), 363–369, DOI: 10.1016/0379-6779(80)90071-5.

42 Q. Meng, Y. Lu, F. Ding, Q. Zhang, L. Chen and Y.-S. Hu, Tuning the Closed Pore Structure of Hard Carbons with the Highest Na Storage Capacity, *ACS Energy Lett.*, 2019, **4**(11), 2608–2612, DOI: 10.1021/acsenergylett.9b01900.

43 V. L. Deringer, C. Merlet, Y. Hu, T. H. Lee, J. A. Kattirtzi, O. Pecher, G. Csányi, S. R. Elliott and C. P. Grey, Towards an Atomistic Understanding of Disordered Carbon Electrode Materials, *Chem. Commun.*, 2018, **54**(47), 5988–5991, DOI: 10.1039/C8CC01388H.

44 Y. Liu, V. I. Artyukhov, M. Liu, A. R. Harutyunyan and B. I. Yakobson, Feasibility of Lithium Storage on Graphene and Its Derivatives, *J. Phys. Chem. Lett.*, 2013, **4**(10), 1737–1742, DOI: 10.1021/JZ400491B.